THE JOURNAL OF PHYSICAL CHEMISTRY B

Article

pubs.acs.org/JPCB

Origin of Decrease in Potency of Darunavir and Two Related Antiviral Inhibitors against HIV-2 Compared to HIV-1 Protease

Parimal Kar and Volker Knecht*

Department of Theory and Bio-Systems, Max Planck Institute of Colloids and Interfaces, Am Mühlenberg 1, 14476 Potsdam, Germany

ABSTRACT: Acquired immune deficiency syndrome (AIDS) is caused by the human immunodeficiency virus (HIV) type 1 and 2 (HIV-1 and HIV-2). HIV-1 is observed worldwide while HIV-2 though prevalent in West Africa is persistently spreading to other parts of the world. An important target for AIDS treatment is the use of HIV protease (PR) inhibitors preventing the replication of the virus. In this work, the popular molecular mechanics Poisson−Boltzmann surface area (MM-PBSA) method has been used to investigate the effectiveness of the HIV-1 PR inhibitors darunavir, GRL-06579A, and GRL-98065 against HIV-2 and HIV-1 protease. The affinity of the inhibitors for both HIV-1 and HIV-2 PR decreases in the order GRL-06579A > darunavir > GRL-98065, in accordance with experimental data. On the other hand, our results show that all these inhibitors bind less strongly to HIV-2 than to HIV-1 protease, again in agreement with experimental findings. The decrease in binding affinity for HIV-2 relative to HIV-1 PR is found to arise from an increase in the energetic penalty from the desolvation of polar groups (DRV) or a decrease in the size of the electrostatic interactions between the inhibitor and the PR (GRL-06579A and GRL-98065). For GRL-98065, also a decrease in the magnitude of the van der Waals interactions contributes to the reduction in binding affinity. A detailed understanding of the molecular forces governing binding and drug resistance might assist in the design of efficient inhibitors against HIV-2 protease.

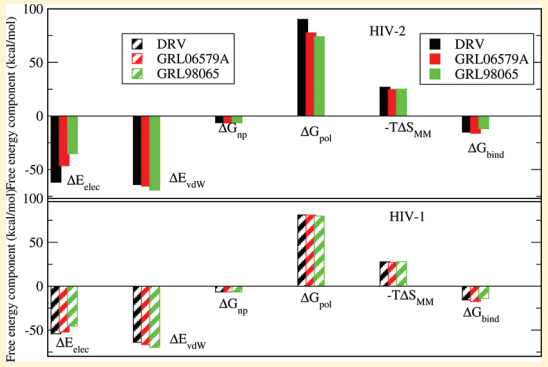

1. INTRODUCTION

According to the UNAIDS 2009 report, ~60 million people worldwide have been infected with acquired immune deficiency syndrome (AIDS) with 25 million deaths.[1] AIDS is caused by human immunodeficiency virus (HIV) type 1 (HIV-1) and type 2 (HIV-2). The World Health Organization (WHO) has declared AIDS to be a pandemic. HIV-1 is observed in worldwide, while HIV-2 is more prevalent in West Africa.[2−4] However, HIV-2 is slowly and persistently spreading to other parts of the world.[4] HIV-2 accounts for 3−8% and 8−10% of AIDS cases in Portugal and Guinea−Bissau, respectively.[5,6] HIV-2 is transmitted in the same manner as HIV-1; however, the frequency of transmission is often reduced as a result of the lower viral loads exhibited in HIV-2 infected patients.[4,7,8] An alarming trend in the AIDS pandemic is the emergence of dual HIV-1/HIV-2 infections, which have been poorly characterized.[4,9] Above all no drug has been developed specifically for HIV-2.

The HIV-2 protease is a homodimer composed of residues 1−99 and 1′−99′ (see Figure 1). Each monomer comprises an α-helix and two antiparallel β-sheets. The active site is evolutionarily conserved and composed of the conserved catalytic triad, Asp25(25′)-Thr26(26′)-Gly27(27′). The Asp dyad, Asp25, and Asp25′ constitute the active site base; it is planar and interacts directly with substrates and inhibitors. HIV-2 protease shares 50% sequence identity with HIV-1 protease, and both have very similar overall structures.[4,10] The two proteases show structural differences at residues 15−20, 30−40, and 65−73 only, regions away from the substrate-binding sites where the homology between the two proteases is low.[11] The wild-type PR2 sequence contains multiple

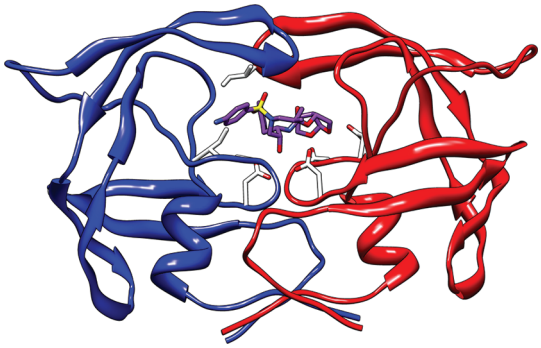

Figure 1. DRV complexed with PR2 dimer. The two subunits of PR2 (1−99 in blue and 1′−99′ in red) are shown in ribbon representation. DRV is shown as a ball and stick representation; colors distinguish between carbon (violet), oxygen (red), nitrogen (blue), and sulfur (yellow). The structures of PR2/GRL-06579A and PR2/GRL-98065 are similar.

Received: December 7, 2011
Revised: January 26, 2012
Published: January 26, 2012

substitutions associated with multidrug resistance (V32I, V82I, etc.) and cross-resistance of HIV-1 to the current protease inhibitors.[4]

HIV type 2 protease (PR2) is responsible for the cleavage of the viral *gag* and *pol* polyproteins into mature, functional proteins. Since inhibition of the PR2 activity prevents the maturation of these viral proteins, and thus the replication of the virus, PR2 has been an important target for anti-AIDS drug therapy. With the introduction of highly active antiretroviral drugs, the treatment of HIV/AIDS patients has been improved, effectively decreasing the mortality rate of HIV/AIDS patients.[12] Developing vaccines to fight the AIDS infection is challenging.[13] Nine HIV-1 protease inhibitors have been approved by the Food and Drug Administration (FDA) for HIV therapy. These drugs are saquinavir (SQV), ritonavir (RTV), indinavir (IDV), nelfinavir (NFV), amprenavir (APV), lopinavir (LPV), atazanavir (AZV), tipranavir (TPV), and darunavir (DRV). However, these drugs are not optimized for the treatment of an HIV-2 infection. Recently Brower et al.[7] have assessed the effectiveness of currently FDA-approved protease inhibitors against the HIV-2 protease. In general, they observe a decrease in potency for the HIV-2 protease compared to the HIV-1 PR by factors ranging between 2 and 80.[7]

In our present work, we have studied the binding of the HIV-1 protease inhibitors darunavir (DRV), GRL-06579A, and GRL-98065 with the HIV-2 protease (PR2). These three inhibitors are highly potent against HIV-1 PR. However, DRV shows 17-fold decreased inhibition for PR2 compared with PR1.[7] GRL-06579A and GRL-98065 show an about 10-fold decreased inhibition of PR2 relative to PR1.[4,7,14] The chemical structures of these inhibitors are shown in Figure 2. Darunavir was designed to target drug-resistant PR1 by introducing more hydrogen bonds with main-chain PR1 atoms compared with older PR1 inhibitors.[4,15] The chemical scaffold of darunavir was used to develop two other inhibitors. Modification of the end groups yields the inhibitors GRL-06579A and GRL-98065. On one end, the aniline moiety is changed to hydroxymethylphenylene in GRL-06579A and to 1,3-benzodioxole in GRL-98065. The unique bis-THF group of DRV remains in the chemical structure of GRL-98065, while a novel substituent hexahydrocyclopenta[b]furan is introduced in GRL-06579A.[4]

To understand the mechanism underlying the binding of HIV-2 protease PR2 to the mentioned inhibitors from an energetic point of view, we have used molecular dynamics simulations and free energy calculations to study the contributions to the binding affinities for the respective complexes. The most rigorous and accurate methods to calculate binding free energies are free energy perturbation (FEP)[16] and thermodynamic integration (TI);[17] however, these methods are computationally very expensive. In contrast, the molecular mechanics Poisson–Boltzmann surface area (MM-PBSA) method[18−20] is faster by several orders of magnitude than FEP or TI. The MM-PBSA scheme is followed in the present study.

In MM-PBSA methods, the binding free energy is estimated as an average of molecular mechanical energies and solvation free energies for an ensemble of configurations of a molecular complex obtained from a trajectory of a molecular dynamics simulation in explicit water. The MM-PB(GB)SA methods have successfully been used to estimate the binding free energy of protein–ligand[21−23] and protein–RNA[24,25] associations. These methods have also been used to study the binding of different inhibitors to protease[26,27] and reverse transcriptase (RT).[28]

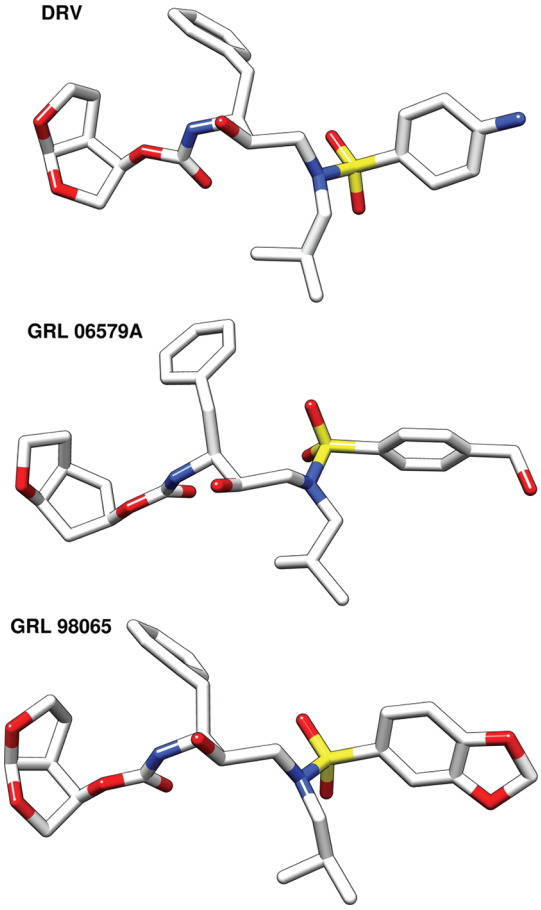

Figure 2. Chemical structure of darunavir, GRL-06579A, and GRL-98065 in stick representation. Colors distinguish between carbon (white), oxygen (red), nitrogen (blue), and sulfur (yellow).

Recently Worch et al.[29] have modeled the interaction propensity of transmembrane domain (TMD) pairs and computed the free energy decrease for TMD dimer formation using the MM-PBSA approach. In contrast to our approach, the PBSA term was replaced with a multiple continua approach established to mimic biomembrane environments with the aqueous phase being modeled by water, the polar head group region by ethanol, and the hydrophobic core by cyclohexane.[30] Höfinger et al. have adopted this multiple continua approach to study the insertion of carbon nanotubes into cellular membranes.[31] The contribution from the change in entropy of the binding partners was obtained from a normal mode analysis of the complex and the individual binding partners.[32,33] The results of our calculations agree well with experimental data and give insight into the origin of the decrease in potency of the inhibitors against HIV-2 protease (PR2) compared to HIV-1 protease (PR1).

2. MATERIALS AND METHODS

The free energies for the formation of HIV protease–inhibitor complexes were evaluated by simulating the corresponding complexes in explicit water and rescoring the free energies of the resulting configurations with an implicit solvent model.

2.1. Structure Generation with Periodic Boundary MD Simulations in Explicit Water. The initial coordinates for our simulations were obtained from the X-ray crystallographic structures of the HIV-2 protease (PR2) complexed with the

dx.doi.org/10.1021/jp211768n | J. Phys. Chem. B 2012, 116, 2605−2614

inhibitors darunavir (DRV), GRL-06579A, and GRL-98065. Recently Kovalevsky and co-workers[4] have determined the X-ray crystallographic structures of the wild-type HIV-2 protease complexed with the three inhibitors at 1.02 Å resolution to analyze the molecular basis for their antiviral potency. The atomic coordinates with the Protein Data Bank accession code 3EBZ for HIV-2 PR2−DRV, 3EC0 for PR2−GRL 06579A, and 3ECG for PR2−GRL 98065 were used for our current study. All crystal water molecules in the crystal structure of the protease−inhibitor complexes were kept in the initial configuration. The proteins were described using the Amber ff99SB force field.[34] The ligand was assigned generalized amber force field (GAFF)[35] atom types, and AM1-BCC[36] atomic charges calculated using the *antechamber*[37] module of Amber.[38] The AM1-BCC charge for an atom is obtained by adding the bond charge correction (BCC) to a semiempirical quantum calculation of the molecular electronic structure according to the Austin Model 1 (AM1) population atomic charge.[39] It has been shown that atomic charges obtained from this charge model emulate the HF/6-31G* electrostatic potential at the surface of a molecule.[36] Our previous work[23] shows that this charge scheme is suitable for this kind of study. The configurations were generated via simulations of the complexes in explicit water. As the protease is located in the cytosol,[40] the standard aqueous environment is appropriate in this case.

The complex was solvated in TIP3P[41] water using a truncated octahedron periodic box, extending at least 10 Å from the complex. Nearly 9500 water molecules were added to solvate the complex and the resulting box size was nearly 90 Å × 90 Å × 90 Å. An appropriate number of chloride ions were added to neutralize the charge of the system. All bond lengths involving hydrogen atoms were constrained using the SHAKE algorithm[42] allowing the usage of a 2 fs time-step. The temperature was kept fixed at 300 K using a Langevin thermostat with a collision frequency of 2 ps^{-1}. The electrostatic interactions were treated with the particle-mesh Ewald (PME) scheme[43] with a fourth-order B-spline interpolation and a tolerance of 10^{-5}. The nonbonded cutoff was 8 Å, and the nonbonded pair list was updated every 50 fs.

Our simulations were conducted according to following protocol: (i) the complex was first optimized by 500 steps of steepest descent followed by another 500 steps of conjugate gradient minimization, keeping all atoms of the complex restrained to their initial positions with weak harmonic restraints. (ii) After the minimization, 50 ps of constant volume MD simulation with 2 kcal·mol^{-1}·$Å^{-2}$ restraints on the atoms of the complex was performed in order to equilibrate the solvent at 300 K without undesirable drifts of the structure. (iii) Next, a 50 ps MD simulation with 2 kcal·mol^{-1}·$Å^{-2}$ restraints on the complex was carried out at a pressure of 1 atm to equilibrate the density using Berendsen's barostat. (iv) Then, the complex was equilibrated for 1 ns without restraint. After the equilibration phase, a 10 ns simulation at constant pressure was conducted and the coordinates were saved every 10 ps, resulting in 1000 configurations for each simulation.

2.2. MM-PBSA Calculations. The protease−inhibitor (P−I) complex formation reaction is represented by the reaction scheme

$$[P]_{aq} + [I]_{aq} \leftrightarrow [PI]_{aq} \tag{1}$$

where all the reactants are assumed to be in aqueous solution. The binding affinity is determined from the free energies of the receptor/protease (P), the ligand/inhibitor (I), and the complex (PI) according to

$$\Delta G_{bind} = G_{PI} - (G_P + G_I) \tag{2}$$

The free energy of each species (P, I, PI) is estimated from

$$G = \langle E_{MM} \rangle + \langle G_{pol} \rangle + \langle G_{np} \rangle - T\langle S_{MM} \rangle \tag{3}$$

Here, E_{MM} is the molecular mechanics gas-phase energy, G_{pol} is the polar and G_{np} the nonpolar solvation free energy of the species, T is the absolute temperature of the system, and S_{MM} is the entropy of the species. The gas-phase molecular mechanics energy E_{MM} can be expressed as

$$E_{MM} = E_{cov} + E_{elec} + E_{vdW} \tag{4}$$

where E_{cov}, E_{elec}, and E_{vdW} denote the contributions from covalent, electrostatic, and van der Waals interactions, respectively. The cutoff radius used in determining E_{elec} is 999 Å, i.e., effectively, all Coulomb interactions were considered. The entropic contributions to the binding free energies arising from changes in the translational (S_{trans}) degrees of freedom at a standard concentration of 1 M, as well as the rotational (S_{rot}) and vibrational (S_{vib}) degrees of freedom, are considered according to

$$S_{MM} = S_{trans} + S_{rot} + S_{vib} \tag{5}$$

The nonpolar solvation free energy (G_{np}) was estimated from[44]

$$G_{np} = \gamma A + b \tag{6}$$

with γ = 0.00542 kcal·mol^{-1}·$Å^{-2}$ and b = 0.92 kcal·mol^{-1}. The symbol A denotes the solvent accessible surface area which was estimated using a probe radius of 1.4 Å with a fast linear combination of pairwise overlap (LCPO) algorithm.[45] The polar solvation free energy G_{pol} was determined by solving the linear Poisson−Boltzmann equation for each configuration.

A common strategy to reduce the noise as well as the computational expense and to cancel errors in simulations is to run molecular dynamics simulations on the complex only. The averages in eq 3 are determined from an ensemble of molecular configurations obtained from such a single trajectory of molecular dynamics simulation. In this single trajectory approach, the covalent energy (E_{cov}) as well as the intramolecular electrostatic and van der Waals energy cancel out in the calculation of ΔG_{bind} which can significantly reduce the noise in most cases.

To account for the specific molecular structure of the water at the binding site, explicit water molecules were included in our free energy calculations. Here, the explicit water molecules were considered as a part of the receptor. Thus, the binding free energy could be obtained from the following equation which is standard MM-PBSA approach for including selected solvent molecules[46]

$$\Delta G_{bind} = \Delta G_{PI+WAT} - (\Delta G_{P+WAT} + \Delta G_I) \tag{7}$$

All the water molecules at the binding always move during a MD simulation. To tackle this problem, for every configuration, the three water molecules closest to the ligand were considered in this calculation.

The total molecular-mechanical energy (E_{gas}) and the covalent energy (E_{cov}) as well as the van der Waals (E_{vdW}) and electrostatic (E_{elec}) components were determined using the parallelized python script *MMPBSA.py.MPI* in Amber-11. This script performs automatically all the required steps to estimate

the binding free energy of protein−ligand complexes using the MM-PBSA method. The electrostatic contribution to the solvation free energy (G_{PB}) was estimated by solving the Poisson−Boltzmann (PB) equation using the Adaptive Poisson−Boltzmann Solver (APBS).[47] In order to solve the PB equation, the grid spacing was set to 0.5 Å in all dimensions and the dielectric constants in the protein or the water were set to 1 or 80, respectively. The ionic strength was set to 0.15 M. The ratio between the longest dimension of the rectangular finite-difference grid, and that of the solute was set to 4.0. The linear PB equation was solved using a maximum of 1000 iterations.

The entropy from the vibrational degrees of freedom was calculated by a normal-mode analysis (NMA) using the Amber *mmpbsa_py_nabnmode* program. To this aim, 200 configurations were selected; each configuration was energy minimized with a Generalized-Born solvent model (nmode_igb = 1) using a maximum of 50 000 steps and a target root-mean-square (rms) gradient of 10^{-4} kcal·mol^{-1}·Å^{-1}.

The standard errors of the mean for the individual components to the binding free energy were computed by dividing the respective standard deviations by the square root of the number of configurations considered. This is reasonable as the autocorrelation time of energy is small compared to the time separation between subsequent configurations chosen here.[48] The standard error of the absolute and the relative binding free energies were evaluated from error propagation.

In order to understand the inhibitor−residue interaction in more detail, the interaction energy was further decomposed into the contributions from each residue of the protease by using the theory of free energy decomposition.[49]

3. RESULTS AND DISCUSSIONS

In order to elucidate the mechanisms underlying the binding of these three different inhibitors to the wild-type protease, an energetic analysis using the MM-PBSA method was conducted. In a first step, the experimental protonation state was estimated.

Experimental Protonation State from pK_a Calculations. In order to pinpoint the likely experimental protonation state, we calculated pK_a values for the Asp25 dyad using PROPKA;[50] the results are shown in Table 1. The predicted

Table 1. pKa Values of Asp25/Asp25′ in the Presence of Inhibitors Obtained from PROPKA[50]

inhibitor	Asp25	Asp25′
PR/DRV	2.19	8.28
PR/GRL 98065	2.13	8.35
PR/GRL 06579A	2.06	8.25

pK_a values are 2.06−2.19 for Asp25 and 8.25−8.35 for Asp25′. Hence, at pH 5.6, where the binding affinities and the structures of the PR2−APV complexes were studied experimentally, Asp25 is most likely ionized and Asp25′ is protonated. Thus, this protonation state is considered in our simulations. Although the active-site Asp residues are related by a symmetric structural dyad in the unbound form, the catalytic mechanism may proceed via asymmetric protonation states.[51]

The catalytic mechanism of HIV-1 PR has been extensively investigated by several approaches.[52] The most widely accepted mechanism for aspartic protease is that described by Suguna et al.[53] The proposed mechanism is based on the crystal structure of the Rhizopys chinensis aspartic protease complexed with a reduced peptide inhibitor. The pH-rate profile of this enzyme implies that only one of the two active site aspartic acids is unprotonated in the active pH range. In the proposed mechanism, the Asp group that is closer to the nucleophilic water molecule was assigned the negative charge. The nucleophilic water molecule held between the catalytic aspartates, after its activation by the negative aspartate side chain, attacks the carbonyl group in the substrate scissile bond to generate an oxyanion tetrahedral intermediate. Protonation of the scissile amide N atom and rearrangement results in the breakdown of the tetrahedral intermediate to the hydrolysis products.

3.1. Stability and Flexibility of the PR2−Inhibitor Complex. Molecular configurations obtained from MD simulations of the complexes in explicit water were used for the calculation of binding free energies. The production simulations of 10 ns carried out for these systems were stable on the basis of the total and potential energies and the root mean square deviation (rmsd) from the X-ray structures. The rms deviations for the backbone atoms from the corresponding X-ray crystal structure in the simulations are shown in Figure 3.

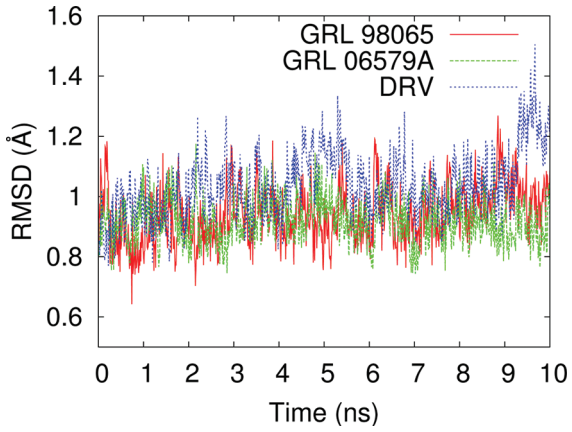

Figure 3. Time evolution of root-mean-square deviations (rmsd) of backbone atoms relative to their positions in experimental structure for wild-type PR2 complexed with three different inhibitors.

The average root mean squared deviations for the backbone atoms from the corresponding X-ray crystal structure in the simulations are 1.16, 1.17, and 1.17 Å for PR2 complexed with DRV, GRL-06579A, and GRL-98065, respectively, with a standard error smaller than 0.17 Å.

A measure for the flexibility of the individual residues is the corresponding B-factors. The B-factors of the individual residues for PR2 complexed with the inhibitors are shown in Figure 4. Overall, the B-factor values of PR2/DRV, PR2/GRL-06579A, and PR2/GRL-98065 are quite similar. This may indicate that different ligands may not lead to significant conformational changes of the PR2 upon binding. Particularly small B-factors are observed for the catalytic dyad (3.23−3.36 Å^2 for Asp25 and 3.46−3.50 Å^2 for Asp25′) for all three complexes. This is expected, as the catalytic function of these residues presumably requires a well-defined stable three-dimensional structure.

As seen from Figure 4, the regions around 17(17′), 40(40′), 65(65′), and 80(80′) show the biggest dynamic fluctuations, i.e, large B-factors. In case of HIV-1 PR, the flexibility of the flap region is crucial to the activity of the protease. A similar trend is observed for PR2. As seen from Figure 4, the flap region,

dx.doi.org/10.1021/jp211768n | J. Phys. Chem. B 2012, 116, 2605−2614

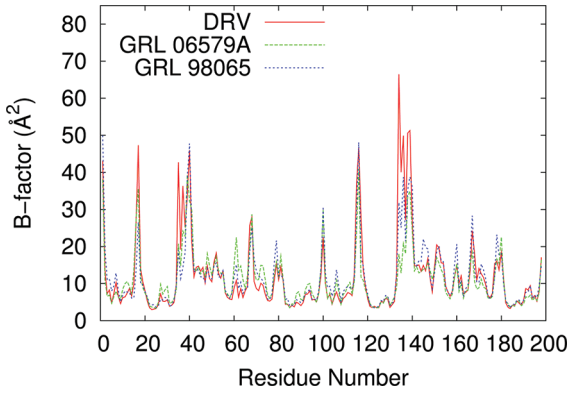

Figure 4. B-factors for HIV-2 protease complexed with darunavir, GRL-06597A, and GRL-98065. Residues 1−99 and 100−198 correspond to residues 1−99 and 1′−99′, respectively.

especially the flap elbow region (37−42), shows significant flexibility. In an earlier study, a similar behavior was observed for HIV-1 PR.[54]

3.2. Binding Free Energies. Tables 2 and 3 give the binding free energies for the association of DRV, GRL-06579A, and GRL-98065 with HIV-2 and HIV-1 protease. The corresponding binding free energies are −15.1, −16.2, and −11.9 kcal·mol^{-1} for HIV-2 PR and −15.7, −17.5, and −11.3 kcal·mol^{-1} for HIV-1 PR, respectively. Thus, for both HIV-1 and HIV-2, the binding affinity decreases in the order GRL-06579A > darunavir > GRL-98065, in agreement with the experimental data. Also, each of the inhibitors binds less strongly to HIV-2 compared to HIV-1 PR, again in accordance with experiment. Most of the binding free energies agree even quantitatively with the experimental values if the statistical errors are considered. Exceptions are DRV/HIV-2 or GRL-98065/HIV-1 where the binding affinities found are somewhat below or above, respectively, the experimental value.

Table 2. Binding Free Energy and Its Components for the Three Inhibitors Complexed with the HIV-2 Protease in kcal·mol^{-1}[a]

component	DRV	GRL-06579A	GRL-98065
ΔE_{elec}	−61.9(0.2)	−46.5(0.3)	−35.3(0.2)
ΔE_{vdW}	−64.1(0.1)	−65.6(0.1)	−69.3(0.1)
ΔG_{np}	−6.3(0.01)	−6.6(0.01)	−6.4(0.01)
ΔG_{pol}	90.3(0.1)	77.7(0.2)	74.1(0.2)
ΔG_{solv}[b]	84.0(0.1)	71.1(0.2)	67.7(0.2)
$\Delta G_{pol,elec}$[c]	28.0(0.2)	31.2(0.5)	32.4(0.3)
$-T\Delta S_{MM}$	26.9(0.4)	24.8(0.5)	25.1(0.4)
ΔG^{sim}_{bind}	−15.1(0.5)	−16.2(0.6)	−11.9(0.5)
ΔG^{exp}_{bind}[d]	−13.4	−15.6	−11.8

[a]Standard errors of the mean are provided in parentheses. [b]$\Delta G_{solv} = \Delta G_{np} + \Delta G_{pol}$. [c]$\Delta G_{pol,elec} = \Delta G_{pol} + \Delta E_{elec}$. [d]Obtained from ref 4.

Table 3. Components of the Binding Free Energy of the Three Inhibitors Complexed with the HIV-1 Protease from Our Calculations[a]

component	DRV	GRL-06579A	GRL-98065
ΔE_{elec}	−54.2(0.3)	−52.3(0.3)	−45.6(0.3)
ΔE_{vdW}	−64.0(0.1)	−66.6(0.1)	−69.7(0.1)
ΔG_{np}	−6.5(0.01)	−6.7(0.01)	−6.6(0.01)
ΔG_{pol}	81.2(0.4)	81.0(0.1)	79.9(0.3)
ΔG_{solv}[b]	74.7(0.4)	74.3(0.2)	73.3(0.2)
$\Delta G_{pol,elec}$[c]	27.0(0.5)	28.7(0.5)	34.3(0.4)
$-T\Delta S_{MM}$	27.8(0.4)	27.1(0.4)	27.9(0.4)
ΔG^{sim}_{bind}	−15.7(0.5)	−17.5(0.6)	−14.1(0.5)
ΔG^{exp}_{bind}[d]	−15.1	−17.0	−13.2

[a]Values are given in kcal·mol^{-1}. Standard errors of the mean are provided in parentheses. [b]$\Delta G_{solv} = \Delta G_{np} + \Delta G_{pol}$. [c]$\Delta G_{pol,elec} = \Delta G_{pol} + \Delta E_{elec}$. [d]Obtained from ref 4.

3.3. Binding Mechanism. In our current study, we are interested to evaluate the relative potency of DRV, GRL-06579A, and GRL-98065 against the wild type and the mutant HIV-2 proteases (PR2) and the molecular basis of drug resistance compared to PR1. In order to elucidate the binding mechanisms, we also provide the individual contributions to the binding free energies. Here, the contribution from the van der Waals or electrostatic interactions between the protease and the inhibitor, ΔE_{vdW} or ΔE_{elec}, respectively, the polar or nonpolar solvation free energy, ΔG_{pol} or G_{np}, respectively, the sum of ΔE_{elec} and ΔG_{pol} denoted as $\Delta G_{pol,elec}$, and the contribution from the configurational entropy of the binding partners, denoted as $-T\Delta S_{MM}$, were considered. The entropic contributions from the vibrational degrees of freedom were calculated using normal-mode analysis.

Energetic Components. The energetics of binding DRV, GRL-06579A, and GRL-98065 to the wild-type PR2 obtained from MM-PBSA calculations are shown in Table 2.

The total binding free energies are found to range between −11.8 and −15.6 kcal·mol^{-1}. The contributions favoring binding are those from the van der Waals interactions between the binding partners (−64.1 to −69.3 kcal·mol^{-1}), the nonpolar interactions with the solvent including the contribution from the hydrophobic effect (−6.3 to −6.6 kcal·mol^{-1}), and the intermolecular electrostatic interactions ΔE_{elec} (−35.3 to −61.9 kcal·mol^{-1}) for all PR2−inhibitor complexes. The most negative value for ΔE_{elec} is found for PR2−DRV (−61.9 kcal·mol^{-1}), followed by PR2−GRL-06579A (−46.5 kcal·mol^{-1}), and PR2−GRL-98065 (−35.3 kcal·mol^{-1}).

Intermolecular electrostatic interactions include contributions from hydrogen bonds, water bridges, and other polar interactions between the protein and the ligand, so the strength of these interactions might be related to the corresponding number of hydrogen bonds and water bridges. PR2−DRV, PR2−GRL-06579A, and PR2−GRL-98065 form five, three, or six intermolecular hydrogen bonds, respectively, and three, two, or three water bridges, correspondingly.[4] All inhibitors show close contacts between their hydroxyethylene OH with the carboxylate side chains of the catalytic residues Asp25 and Asp25′. The OH group forms two short contacts of 2.5−2.6 Å to the outer $O^{\delta 2}$ of Asp25 and the inner $O^{\delta 1}$ of Asp25′. The latter distance is increased to 2.8 Å for PR2−GRL-98065.[4] This structural feature presumably contributes to the fact that the electrostatic interactions of this inhibitor with PR2 are weaker compared to the two other inhibitors as found here. On the other hand, the finding that ΔE_{elec} is more negative for PR2−DRV than for PR2−GRL-06579A correlates well with the fact that the former exhibits two more hydrogen bonds and one more water bridge with PR2 than the latter.

The PR2 inhibitors are quite polar molecules which is reflected in a large number of polar interactions with PR2 evident from structural inspection and strong electrostatic interactions revealed from our calculations. It is illustrative to compare the strength of the electrostatic contribution to the affinity of the PR2−inhibitor complexes to the value observed

dx.doi.org/10.1021/jp211768n | J. Phys. Chem. B 2012, 116, 2605−2614

for the affinity of a lipid molecule, the steroid progesterone (PRG), for the progesterone antibody DB3. PRG is largely hydrophobic; the only hydrophilic groups of this ligand are two carbonyl groups, each forming a hydrogen bond with the antibody. For DB3−PRG, ΔE_{elec} is found to be −17.5 kcal·mol^{-1}.[23] This is smaller than the values for the PR2−inhibitors observed here by more than a factor of 2, correlating well with the smaller number of hydrogen bonds for DB3−PRG compared to the PR2−inhibitor complexes.

Association is opposed by an unfavorable desolvation of polar groups (ΔG_{pol}), yielding a contribution of 74.1−90.3 kcal·mol^{-1} for all PR2−inhibitor complexes. As found for other systems,[21,23,55,56] the unfavorable desolvation of polar groups is only partially compensated by favorable intermolecular electrostatic interactions. The sum of the contribution from the desolvation of polar groups and the intermolecular electrostatic interactions varies from 28.0 to 32.4 kcal·mol^{-1} for the protease−inhibitor complexes. Interestingly, the size of ΔE_{elec} correlates with the magnitude of ΔG_{pol} and anticorrelates with the size of the contribution from the intermolecular van der Waals interactions ΔE_{vdw}, such that changes in ΔE_{elec} are partially compensated by changes in ΔG_{pol} and ΔE_{vdw}. In contrast, for the binding of the steroid 5β-androstane-3,17-dione (5AD) to the catalytic antibody 1E9, the size of ΔE_{elec} has been found to anticorrelate with the magnitude of ΔG_{pol}.[23] For the 1E9−5AD and L^{47H}W/R0^{100H}W 1E9−5AD complexes, the intermolecular electrostatic energies were −9.4 and −10.7 kcal·mol^{-1}, respectively, while the polar solvation free energies were 28.2 and 26.8 kcal·mol^{-1}, respectively.[23]

Formation of macromolecular complexes is in general opposed by a loss in configurational entropy of the binding partners.[23,48,55] The corresponding contributions from the loss in entropy due to the translational, rotational, and vibrational degrees of freedom to the binding of free energy of the protease−inhibitor complexes were in the range 24.8−26.9 kcal·mol^{-1}. Interestingly, the entropic effects appear to be pretty large here compared to complexes of the Diels−Alderase antibody 1E9 with two different steroids we have studied earlier.[23] The large entropic effect may arise from the conformational freedom of the ligands which exhibit 13 rotatable bonds each. The rotation around these bonds will be more restricted in the presence than in the absence of the protease, leading to a decrease in the entropy upon binding. Compared to the ligands considered here, steroids are quite rigid; the ones considered in our earlier work exhibited at most one rotatable bond. Hence, indeed, the entropic component for the binding free energy of the 1E9−steroid complexes (about 15 kcal·mol^{-1}) was much smaller than that for the protease−inhibitor complexes studied here (25−27 kcal·mol^{-1}).

PR2−GRL-06579A versus PR2−DRV. For the PR2−GRL-06579A complex, the binding free energy ΔG_{bind} is more favorable than ΔG_{bind} for PR2−DRV by −2.2 kcal·mol^{-1}. For the PR2−GRL-06579A complex, the intermolecular van der Waals interaction energy is shifted compared to PR2−DRV by −1.5 kcal·mol^{-1}. However, the gas phase electrostatic energy ΔE_{elec} in the PR2−GRL-06579A complex is changed relative to that of PR2−DRV by 15.4 kcal·mol^{-1}. Considering ΔE_{elec} alone one could thus expect that the DRV would be more potent against PR2 than GRL-06579A. In contrast, we see that GRL-06579A is more potent than DRV. This is because of the lower polar solvation free energy for PR2−GRL-06579A compared to PR2−DRV.

PR2−GRL-98065 versus PR2−GRL-06579A. It is evident from Table 2 that the inhibitor GRL-06579A is much more potent against PR2 compared to the inhibitor GRL-98065, although the contributions from ΔE_{vdW}, ΔG_{np}, and ΔG_{pol} are more favorable for GRL-98065 relative to GRL-06579A. The van der Waals interaction energy ΔE_{vdW} is shifted by −3.7 kcal·mol^{-1} for GRL-98065 relative to GRL-06579A. There is a minor shift of +0.2 kcal·mol^{-1} in the nonpolar solvation free energy for GRL-98065 compared to GRL-06579A. For the PR2−GRL-98065 complex, the polar solvation free energy is changed by −6.6 kcal·mol^{-1} relative to PR2−GRL-06579A. For the PR2−GRL-98065 complex, the intermolecular electrostatic energy ΔE_{elec} is decreased in size by 11.2 kcal·mol^{-1}. The increase in the magnitude of ΔE_{vdW} and the decrease in ΔG_{pol} are not sufficient to counter the decrease in the size of ΔE_{elec}. Hence, we observe a less negative binding free energy for GRL-98065 compared to GRL-06579A.

PR2−DRV versus PR2−GRL-98065. Experimental results suggest that the inhibitor DRV is more potent against PR2 than GRL-98065.[4] Our calculations agree well with this experimental observation (see Table 2). Our calculations yield a binding free energy of −15.1 kcal·mol^{-1} for PR2−DRV while a binding free energy of −11.9 kcal·mol^{-1} is obtained for the complex PR2−GRL-98065. For the PR2−GRL-98065 complex, the intermolecular van der Waals interaction energy is shifted by −5.2 kcal·mol^{-1} compared to PR2−DRV. The polar solvation free energy is more favorable for GRL-98065 compared to DRV, being shifted by −16.2 kcal·mol^{-1} for GRL-98065 relative to DRV. However, the gas phase electrostatic energy ΔE_{elec} in PR2−GRL-98065 is shifted by 26.6 kcal·mol^{-1} relative to that of PR2−DRV. Hence, the favorable shifts in ΔE_{vdW} and ΔG_{pol} are not sufficient to counter the decrease in the size of ΔE_{elec} which is the reason why GRL-98065 is less potent against PR2 compared to DRV.

3.4. PR1−Inhibitor versus PR2−Inhibitor Complexes.

To compare the components of the binding free energies for the PR2−inhibitor with the PR1−inhibitor complexes, all three inhibitors bound to the HIV-1 protease were also simulated. The same protocols were followed as we did for the PR2−inhibitor complexes. The binding and mutation induced drug resistance of the PR1−DRV and PR1−GRL-98065 complexes were studied previously.[56,57] However, the PR1−GRL-06579A complex was not investigated earlier. The binding free energies obtained from their calculations are −26.78 and −19.02 kcal·mol^{-1} for PR1/DRV and PR1/GRL-98065, respectively, while the corresponding experimental binding free energies are −15.1 and −13.2 kcal·mol^{-1}. On the other hand, predicted binding free energies for PR1/DRV and PR1/GRL-98065 from our calculations are −15.7 and −14.1 kcal·mol^{-1}, respectively. Our results match better with experimental data compared to previous results.

PR1/DRV versus PR2/DRV. Experimentally DRV shows a 17-fold decreased potency against PR2 compared to PR1.[4] This is in agreement with our calculations (see Tables 2 and 3). The binding mechanism is the same for both cases. Comparing the components of the binding free energy of PR1−DRV and PR2−DRV gives insights into the origin of the decrease in the size of the binding free energy for PR2−DRV compared to PR1−DRV. For PR2−DRV, the intermolecular electrostatic energy ΔE_{elec} is more favorable than for PR1−DRV, being shifted by −7.7 kcal·mol^{-1} compared to the latter. However, the van der Waals interaction energy remains the same for both complexes. The nonpolar component of the solvation free

energy does not change much for both complexes either. However, the polar solvation free energy, which unfavors the complex formation, is less unfavorable for PR1−DRV compared to PR2−DRV. For the PR1−DRV complex, the polar solvation free energy is shifted by −9.1 kcal·mol^{-1} compared to PR2−DRV. The increase in the size of the gas phase electrostatic energy ΔE_{elec} in PR2−DRV is hence not sufficient to counter the increase in the polar solvation free energy. Hence, DRV is more potent against PR1 compared to PR2. The reduced potency against PR2 is mainly due to the increase in the polar solvation free energy.

PR1/GRL-06579A versus PR2/GRL-06579A. It is evident from Tables 2 and 3 that GRL-06579A is more potent against PR1 compared to PR2. The intermolecular electrostatic and van der Waals interaction energies are less favorable in the case of PR2−GRL-06579A compared to PR1−GRL-06579A. The polar solvation free energy is less unfavorable in the case of PR2−GRL-06579A compared to PR1−GRL-06579A. However, the decrease in the polar solvation free energy for PR2−GRL-06579A is not sufficient to compensate the decrease in the size of the electrostatic and van der Waals energies, leading to the decrease in the magnitude of the binding free energy compared to PR1. For PR2, the electrostatic and van der Waals energies are shifted by 5.8 and 1.0 kcal·mol^{-1}, respectively, compared to PR1. There is a change of −3.3 kcal·mol^{-1} in ΔG_{pol} for PR2 relative to PR1. The entropic contribution to the binding free energy is less unfavorable for PR1 in comparison to PR2, a shift of −2.3 kcal·mol^{-1} being observed for PR2 relative to PR1. The decrease in potency thus mainly arises due to the reduced magnitude of the intermolecular electrostatic energy.

PR1/GRL-98065 versus PR2/GRL-98065. Compared to PR1, GRL-98065 has been shown to exhibit a ∼10-fold lower potency against PR2.[4] The comparison of energetic components of the free energy between PR1/GRL-98065 and PR2/GRL-98065 provides molecular insights into the cause of the reduced potency observed for PR2 compared to PR1. For PR2, the sizes of the intermolecular electrostatic (ΔE_{elec}) and van der Waals interaction energies (ΔE_{vdW}) are decreased by 10.3 and 0.4 kcal·mol^{-1}, respectively, compared to PR1. The polar component of the solvation free energy is shifted by −5.8 kcal·mol^{-1} relative to PR1. However, the favorable change in the polar solvation free energy is not sufficient to compensate the unfavorable shifts of ΔE_{elec} and ΔE_{vdW}, explaining the decrease in potency against PR2 compared to PR1.

3.5. Decomposition of Binding Free Energy into Contributions from Individual Residues. To acquire more detailed insights into the underlying binding mechanisms, the binding free energies were further decomposed into contributions from individual residues to generate an inhibitor−residue interaction spectrum as shown in Figure 5. This is extremely useful to understand the drug binding mechanism of DRV, GRL-06579A, and GRL-98065 to PR2 at the atomic level. From Figure 5, it is clear that the overall interaction spectra of all the complexes are quite similar. The attractive contributions mainly come from six groups around Ala28/Ala28′, Ile50/Ile50′, and Ile84/Ile84′.

Table 4 reports the decomposition of ΔG_{bind} on a per-residue basis into contributions from van der Waals and electrostatic interactions, as well as polar and nonpolar solvation energies for residues with $|\Delta G| \geq 1.5$ kcal·mol^{-1} for the three complexes. These residues include Ala28 and Ile50′ forming contacts with the benzene ring shown on the right of Figure 2 (top, middle, and bottom). The decomposition of ΔG_{bind} was carried out using the MM-GBSA scheme. For all eight residues, the van der Waals energy and the nonpolar solvation free energy drive the binding of the inhibitor to PR2. For all the three complexes, the most significant contributions to the binding free energy come from Ala28 and Ala28′. Ala28 contributes −2.92, −2.28, and −2.26 kcal·mol^{-1} to the binding free energy for PR2/DRV, PR2/GRL-06579A, and PR2/GRL-98065, respectively. Most of the contributions of Ala28 derive from the van der Waals interactions. For Ala28, the backbone contributes more favorably than the side chain and the contributions from the backbone are −2.44, −1.61, and −1.65 kcal·mol^{-1} for PR2/DRV, PR2/GRL-06579A, and PR2/GRL-98065, correspondingly.

For all the three complexes, the contribution from Ala28′ is more favorable compared to Ala28. Ala28′ contributes −4.38, −2.99, and −3.93 kcal·mol^{-1} for PR2/DRV, PR2/GRL-

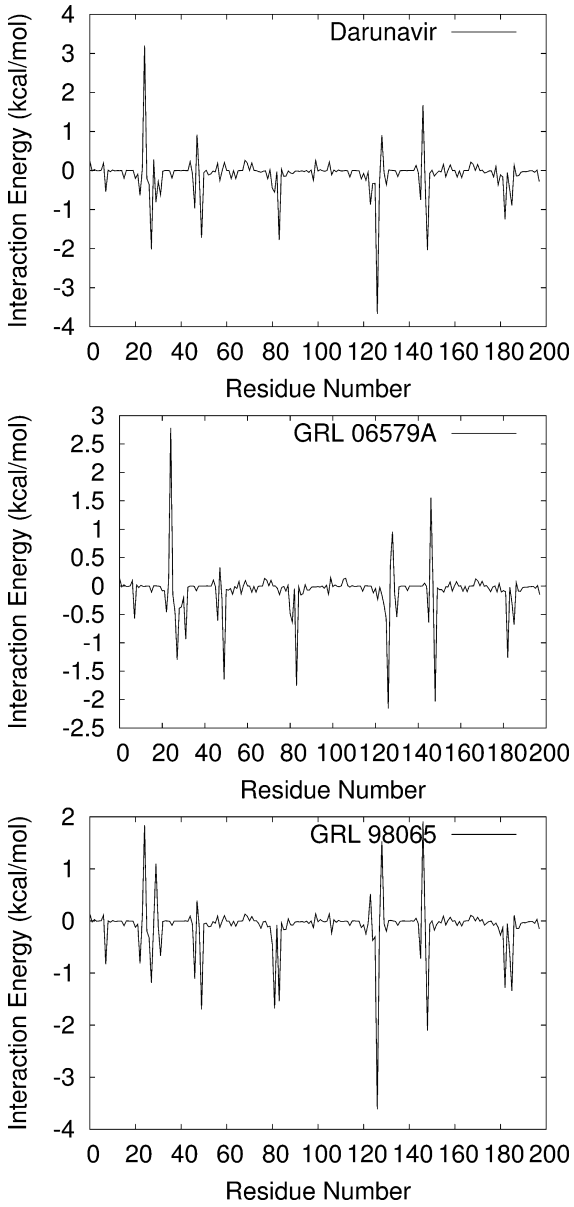

Figure 5. Decomposition of binding free energies for the PR2−inhibitors complexes into contributions from individual residues. Residues 1−99 correspond to chain A and 100−198 to chain B of the PR2.

dx.doi.org/10.1021/jp211768n | J. Phys. Chem. B 2012, 116, 2605−2614

Table 4. Decomposition of Binding Free Energies for the PR2−Inhibitor Complexes into Contributions from Individual Residues[a]

residue	T_{vdW}	T_{ele}	T_{GB}	T_{np}	T_S	T_B	T_{TOT}
PR2/DRV							
Ala28	−2.04	−0.09	−0.65	−0.14	−0.48	−2.44	−2.92
Gly49	−0.50	−2.23	1.24	−0.07	0.00	−1.56	−1.56
Ile50	−1.87	−0.53	0.42	−0.21	−1.81	−0.38	−2.19
Ile84	−1.54	−0.06	0.08	−0.13	−1.54	−0.11	−1.65
Asp25′	−0.16	−2.78	0.59	−0.08	−2.43	0.00	−2.43
Ala28′	−2.40	−2.60	0.78	−0.15	−0.59	−3.79	−4.38
Gly49′	−0.98	−1.96	1.50	−0.11	0.00	−1.54	−1.54
Ile50′	−2.42	−1.25	1.21	−0.20	−2.08	−0.58	−2.66
PR2/GRL-06579A							
Ala28	−1.62	0.06	−0.55	−0.17	−0.67	−1.61	−2.28
Ile50	−1.75	−0.44	0.34	−0.16	−1.68	−0.33	−2.01
Ile84	−1.85	−0.03	0.00	−0.17	−1.91	−0.13	−2.04
Gly27′	−0.97	−0.20	−0.29	−0.08	0.00	−1.54	−1.54
Ala28′	−2.23	−0.96	0.34	−0.16	−0.63	−2.36	−2.99
Gly49′	−1.21	−2.05	1.61	−0.12	0.00	−1.77	−1.77
Ile50′	−2.74	−1.22	1.18	−0.21	−2.33	−0.65	−2.98
Ile84′	−1.42	0.08	−0.08	−0.14	−1.46	−0.09	−1.55
PR2/GRL-98065							
Ala28	−1.80	0.32	−0.60	−0.17	−0.61	−1.65	−2.26
Ile50	−1.65	−0.22	0.19	−0.14	−1.54	−0.28	−1.82
Ile82	−1.55	−0.10	0.21	−0.20	−1.55	−0.09	−1.64
Ile84	−1.58	0.05	−0.09	−0.14	−1.63	−0.13	−1.76
Gly27′	−1.21	−0.13	−0.06	−0.10	0.00	−1.50	−1.50
Ala28′	−2.38	−1.86	0.47	−0.16	−0.60	−3.33	−3.93
Gly49′	−1.27	−1.74	1.54	−0.15	0.00	−1.61	−1.61
Ile50′	−2.36	−1.23	1.08	−0.18	−1.98	−0.72	−2.70

[a]The contributions from the van der Waals (T_{vdW}) and electrostatic interactions (T_{ele}), as well as the polar (T_{GB}) and nonpolar solvation energy (T_{np}), and the total contribution of a given residue (T_{TOT}), are shown. T_S and T_B represent the backbone and side chain contributions. Only residues with $|T_{TOT}| \geq 1.5$ kcal·mol^{-1} were listed. All values are given in kcal·mol^{-1}.

06579A, and PR2/GRL 98065, respectively. In the case of PR2/GRL-06579A and PR2/GRL-98065, most of the contributions from Ala28′ derive from the van der Waals interactions while the electrostatic interactions provide the most favorable contribution to the binding free energy for PR2/DRV. Similar to Ala28, most of the contribution of Ala28′ comes from the backbone. Ile50 and Ile50′ also provide large contributions to the binding free energy varying in the range −1.82 to −2.98 kcal·mol^{-1}. Unlike Ala28/Ala28′ contributing largely via their backbones, Ile50 and Ile50′ contribute largely by their side chains (van der Waals interactions) to the binding. The contributions of Gly49′ are found in the range −1.54 to −1.77 kcal·mol^{-1}, and most of the contributions originate from the electrostatic interactions. As shown in Table 4, for all the three complexes, Ile84 yields a greater contribution from its side chain than from its backbone, mainly due to van der Waals interactions. The total contributions of Ile84 for the three complexes are found in the range −1.56 to −2.04 kcal·mol^{-1}.

Contribution of Aspartic Dyad to Binding Free Energies. The catalytic aspartic dyad Asp25/Asp25′ is expected to be crucial to the binding of inhibitors with the protease. Hence it is important to estimate the total contribution coming from the Asp25 dyad to the binding free energy. The contributions from Asp25/Asp25′ to the binding free energy are provided in Table 5. We found the total contributions from Asp25/Asp25′ to be attractive varying in the range −1.93 to −2.84 kcal·mol^{-1} for all three PR2−inhibitor complexes. The individual contributions from the two Asp residues to the binding free energy are given

Table 5. Contribution to the Binding Free Energy from the Asp25′/Asp25′ Dyad in kcal·mol^{-1}

complex	Asp25	Asp25′	total
PR2/DRV	−0.41	−2.43	−2.84
PR2/GRL-98065	−1.33	−0.90	−2.23
PR2/GRL-06579A	−0.85	−1.08	−1.93

in the following. For the PR2/DRV system, both Asp25 and Asp25′ contribute favorably, and the contribution from Asp25′ (−2.43 kcal·mol^{-1}) is almost six times that of Asp25 (−0.41 kcal·mol^{-1}). For the PR2/GRL-06579A system, both Asp25 and Asp25′ are attractive, Asp25′ being more attractive (−1.08 kcal·mol^{-1}) than Asp25 (−0.85 kcal·mol^{-1}). For the PR2/GRL-98065 complex, Asp25 yields a favorable contribution of −1.33 kcal·mol^{-1} while the contribution from Asp25′ is −0.90 kcal·mol^{-1}. Only for PR2/GRL-98065, Asp25 is more attractive than Asp25′.

Table 5 shows that that the magnitude of the total contribution from Asp25/Asp25′ to the binding free energy is the smallest (−1.93 kcal·mol^{-1}) for the PR2/GRL-06579A complex, while the largest (−2.84 kcal·mol^{-1}) contribution is found for the PR2/DRV complex. For the PR2/GRL-98065 complex, an intermediate contribution of −2.23 kcal·mol^{-1} is found. For the PR2/GRL-06579A complex, interestingly, the total binding free energy ΔG_{bind} is the largest (−15.6 kcal·mol^{-1}) while the contribution from Asp25/Asp25′ to the binding free energy is the least in size (−1.93 kcal·mol^{-1}).

dx.doi.org/10.1021/jp211768n | J. Phys. Chem. B 2012, 116, 2605−2614

4. CONCLUSION

In the present work, we have studied the binding of HIV-2 protease to darunavir, GRL-06579A, and GRL-98065 using a combination of 10-ns MD simulations in explicit water and implicit solvent-free energy calculations. Our calculations show that all three inhibitors exhibit a decreased potency against PR2 compared to PR1 in agreement with experiments. The potencies of these inhibitors against PR2 decrease in the order GRL-06579A > DRV > GRL-98065. On the other hand, our results show that all these inhibitors bind less strongly to HIV-2 than to HIV-1 protease, again in agreement with experimental findings. The decrease in binding affinity for HIV-2 relative to HIV-1 PR is found to arise from an increase in the energetic penalty from the desolvation of polar groups (DRV), or a decrease in the size of the electrostatic interactions between the inhibitor and the PR (GRL-06579A and GRL-98065). For GRL-98065, also a decrease in the magnitude of the van der Waals interactions contributes to the reduction in binding affinity. For all PR2−inhibitor complexes, binding is mainly driven by the favorable contributions from the intermolecular van der Waals and electrostatic interactions, as well as the nonpolar component of the solvation free energy. This is similar to what has been observed for other systems. The complex formation is opposed by the polar solvation free energy and entropy. Our study reveals that GRL-06579A is more potent than DRV because of the decreased unfavorable contribution from the polar solvation free energy compared to DRV. GRL-06579A is also more potent than GRL-98065 due to an increased contribution from the intermolecular electrostatic interactions in the case of PR2−GRL-06579A compared to PR2−GRL-98065. Our findings might assist in the design of new drugs optimized for the HIV-2 protease.

AUTHOR INFORMATION

Corresponding Author

*E-mail: Volker.Knecht@mpikg.mpg.de. Phone: +49-331-5679732. Fax: +49-331-5679612.

Notes

The authors declare no competing financial interest.

ACKNOWLEDGMENTS

This work was supported by the Federal Ministry of Education and Research (BMBF), Germany. P.K. acknowledges the support from the German Research Foundation (DFG) in the framework of the International Research Training Group 1524.

REFERENCES

(1) UNAIDS. UNAIDS publication series; 2009.
(2) Bock, P. J.; Markovitz, D. M. *AIDS* **2001**, *15*, S35−S45.
(3) Kanki, P. J.; De Cock, K. M. *AIDS* **1994**, *8*, S85−S93.
(4) Kovalevsky, A. Y.; Louis, J. M.; Aniana, A.; Ghosh, A. K.; Weber, I. T.. *J. Mol. Biol.* **2008**, *384*, 178−192.
(5) Gomes, P.; Abecasis, A.; Almeida, M.; Camacho, R.; Mansinho, K. *Lancet Infect. Dis.* **2003**, *3*, 683−684.
(6) Wilkins, A.; Ricard, D.; Todd, J.; Whittle, H.; Dias, F.; Paulo Da Silva, A. *AIDS* **1993**, *7*, 1119−1122.
(7) Brower, E. T.; Bacha, U. M.; Kawasaki, Y.; Freire, E. *Chem. Biol. Drug Des.* **2008**, *71*, 298−305.
(8) Marlink, R.; Kanki, P. J.; Thior, I.; Travers, K.; Eisen, G.; Siby, T.; Traore, I; Hsieh, C. C.; Dia, M. C.; Gueye, E.; Hellinger, J.; Gueyendiaye, A.; Sankale, J. L.; Ndoye, I.; Mboup, S.; Essex, M. *Science* **1994**, *265*, 1587−1590.
(9) Sarr, A. D.; Sankale, J. L.; Gueye-Ndiaye, A.; Essex, M.; Mboup, S.; Kanki, P. J. *AIDS Res. Hum. Retroviruses* **2000**, *16*, 295−298.
(10) Gustchina, A.; Weber, I. T. *Proteins* **1991**, *10*, 325−339.
(11) Tong, L.; Pav, S.; Pargellis, C.; Do, F.; Lamarre, D.; Anderson, P. C. *Proc. Natl. Acad. Sci. U.S.A.* **1993**, *90*, 8387−8391.
(12) Wood, E.; Hogg, R. S.; Yip, B.; Moore, D.; Harringan, P. R.; Montaner, J. S. *HIV Med.* **2007**, *8*, 80−85.
(13) Walker, B. D.; Burton, D. R. *Science* **2008**, *320*, 760−764.
(14) Amano, M.; Koh, Y.; Das, D.; Li, J.; Leshchenko, S.; Wang, Y.-F.; Boross, P. I.; Weber, I. T.; Ghosh, A. K.; Mitsuya, H. *Antimicrob. Agents Chemother.* **2007**, *51*, 2143−2155.
(15) Ghosh, A. K.; Chapsal, B. D.; Weber, I. T.; Mitsua, H. *Acc. Chem. Res.* **2008**, *41*, 78−86.
(16) Kollman, P. A. *Chem. Rev.* **1993**, *93*, 2395−2417.
(17) Lybrand, T.; McCammon, J. A.; Wipff, G. *Proc. Natl. Acad. Sci. U.S.A.* **1986**, *83*, 833−835.
(18) Jayaram, B.; Sprous, D.; Young, M. A.; Beveridge, D. L. *J. Am. Chem. Soc.* **1998**, *120*, 10629−10633.
(19) Vorobjev, Y. N.; Almagro, J. C.; Hermans, J. *Proteins* **1998**, *32*, 399−413.
(20) Kollman, P. A.; Massova, I.; Reyes, C.; Kuhn, B.; Huo, S.; Chong, L.; Lee, M.; Lee, T.; Duan, Y.; Wang, W.; Donini, O.; Cieplak, P.; Srinivasan, J.; Case, D. A.; Cheatham, T. E. *Acc. Chem. Res.* **2000**, *33*, 889−897.
(21) Kuhn, B.; Kollman, P. A. *J. Med. Chem.* **2000**, *43*, 3786−3791.
(22) Rastelli, G.; Rio, A. D.; Degliesposti, G.; Sgobba, M. *J. Comput. Chem.* **2010**, *31*, 797−810.
(23) Kar, P.; Lipowsky, R.; Knecht, V. *J. Phys. Chem. B* **2011**, *115*, 7661−7669.
(24) Reyes, C. M.; Kollman, P. A. *J. Mol. Biol.* **2000**, *295*, 1−6.
(25) Reyes, C. M.; Kollman, P. A. *J. Mol. Biol.* **2000**, *297*, 1145−1158.
(26) Chen, X.; Weber, I. T.; Harrison, R. W. *J. Mol. Model.* **2004**, *10*, 373−381.
(27) Hou, T.; McLaughlin, W. A.; Wang, W. *Proteins* **2007**, *71*, 1163−1174.
(28) Wang, J.; Morin, P.; Wang, W.; Kollman, P. A. *J. Am. Chem. Soc.* **2001**, *123*, 5221−5230.
(29) Worch, R.; Bökel, C.; Höfinger, S.; Schwille, P.; Weidemann, T. *Proteomics* **2010**, *10*, 4196−4208.
(30) Kar, P.; Seel, M.; Weidemann, T.; Höfinger, S. *FEBS Lett.* **2009**, *583*, 1909−1915.
(31) Höfinger, S.; Melle-Franco, M.; Gallo, T.; Cantelli, A.; Calvaresi, M.; Gomes, J. A. N. F.; Zerbetto, F. *Biomaterials* **2011**, *32*, 7079−7085.
(32) Karplus, M.; Kushick, J. N. *Macromolecules* **1981**, *14*, 325−332.
(33) Rempe, S. B.; Jonsson, H. *Chem. Educ.* **1998**, *3*, 1−17.
(34) Hornak, V.; Abel, R.; Okur, A.; Strockbine, B.; Roitberg, A.; Simmerling, C. *Proteins* **2006**, *65*, 712−725.
(35) Wang, J.; Wolf, R. M.; Caldwell, J. W.; Kollman, P. A.; Case, D. A. *J. Comput. Chem.* **2004**, *25*, 1157−1174.
(36) Jakalian, A.; Jack, D. B.; Bayly, C. I. *J. Comput. Chem.* **2002**, *23*, 1623−1641.
(37) Wang, J.; Wang, W.; Kollman, P. A.; Case, D. A. *J. Mol. Graph. Mod.* **2006**, *25*, 247−260.
(38) Case, D. A.; Cheatham, T.; Darden, T.; Gohlke, H.; Luo, R.; Merz, K. M.; Onufriev, A. Jr.; Simmerling, C.; Wang, B.; Woods, R. *J. Computat. Chem.* **2005**, *26*, 1668−1688.
(39) Dewar, M. J. S.; Zoebisch, E. G.; Healy, E. F.; Stewart, J. J. P. *J. Am. Chem. Soc.* **1985**, *107*, 3902−3909.
(40) Bren, G. D.; Whitman, J.; Cummins, N.; Shepard, B.; Rizza, S. A.; Trushin, S. A.; Badley, A. D. *PLoS ONE* **2008**, *3*, e2112.
(41) Jorgensen, W. L.; Chandrasekar, J.; Madura, J. D.; Impey, R.; Klein, K. *J. Chem. Phys.* **1983**, *79*, 926−935.
(42) Ryckaert, J.-P.; Ciccotti, G.; Berendsen, H. J. C. *J. Comput. Phys.* **1977**, *23*, 327−341.
(43) Darden, T.; York, D.; Pedersen, L. *J. Chem. Phys.* **1993**, *98*, 10089−10092.
(44) Sitkoff, D.; Sharp, K. A.; Honig, B. *J. Phys. Chem.* **1994**, *98*, 1978−1988.

(45) Weise, J.; Shenkin, P. S.; Still, W. C. *J. Comput. Chem.* **1999**, *20*, 217−230.
(46) Treesuwan, W.; Hannongbua, S. *J. Mol. Graph. Model.* **2009**, *27*, 921−929.
(47) Baker, N. A.; Sept, D.; Joseph, S.; Holst, M. J.; McCammon, J. A. *Proc. Natl. Acad. Sci. U.S.A.* **2001**, *98*, 10037−10041.
(48) Knecht, V. *J. Phys. Chem. B* **2010**, *114*, 12701−12707.
(49) Gohlke, H.; Kiel, C.; Case, D. A. *J. Mol. Biol.* **2003**, *330*, 891−913.
(50) Li, H.; Robertson, A. D.; Jensen, J. H. *Proteins* **2005**, *61*, 704−721.
(51) Adachi, M.; Ohhara, T.; Kurihara, K.; Tamada, T.; Honjo, E.; Okazaki, N.; Arai, S.; Shoyama, Y.; Kimura, K.; Matsumura, H.; Sugiyama, S.; Adachi, H.; Takano, K.; Mori, Y.; Hidaka, K.; Kimura, T.; Hayashi, Y.; Kiso, Y.; Kuroki, R. *Proc. Natl. Acad. Sci. U.S.A.* **2009**, *106*, 4641−4646.
(52) Brik, A.; Wong, C. H. *Org. Biomol. Chem.* **2003**, *1*, 5−14.
(53) Suguna, K.; Padlan, E. A.; Smith, C. W.; Carlson, W. D.; Davies, D. R. *Proc. Natl. Acad. Sci. U.S.A.* **1987**, *84*, 7009−7013.
(54) Zhu, Z. W.; Schuster, D. I.; Tuckerman, M. E. *Biochemistry* **2003**, *42*, 1326−1333.
(55) Chong, L. T.; Duan, Y.; Wang, L.; Massova, I.; Kollman, P. A. *Proc. Natl. Acad. Sci. U.S.A.* **1999**, *96*, 14330−14335.
(56) Chen, J.; Zhang, S.; Liu, X.; Zhang, Q. *J. Mol. Model.* **2010**, *16*, 459−468.
(57) Hu, G.-D.; Zhu, T.; Zhang, S.-L.; Wang, D.; Zhang, Q.-G. *Eur. J. Med. Chem.* **2010**, *45*, 227−235.